Structure-derived electronic and optical properties of transparent conducting oxides

David Segev and Su-Huai Wei
National Renewable Energy Laboratory, Golden, Colorado 80401, USA
(Received 15 October 2004; revised manuscript received 28 December 2004; published 29 March 2005)

Using the first-principles method, we have studied the stability and electronic band structures of the transparent conducting oxides $SnZn_2O_4$, $SnCd_2O_4$, and $CdIn_2O_4$. Our calculated lowest-energy phases of these compounds are similar to those found experimentally. However, we find an orthorhombic structure of $SnZn_2O_4$, which is close in energy to the inverse spinel structure, and a new "inverse" orthorhombic structure for $CdIn_2O_4$, with an energy close to that of the inverse spinel structure. The stability of these compounds can be explained by the Coulomb energy, atomic size, and chemical character of the constituent elements. We analyze the chemical character of the band edges and explain the general trend observed in the fundamental band gap and energy difference between the first and second conduction bands. The latter is found to be large for the thermodynamically stable structures, which explains the transparency of these *n*-type conducting oxides. Based on these analyses, we derive general rules for designing more efficient transparent conducting oxides. We have also calculated the Moss-Burstein electron effective masses and the optical transition matrix elements of these compounds. We find that transitions between the valence band maximum and the conduction band minimum are forbidden by symmetry, and that the optical gaps are about 1 eV larger than the corresponding fundamental band gaps. The same forbidden transitions are found between the first and second conduction bands. Our calculated dependence of the absorption spectrum on the carrier concentration reveals new features for *n*-type doped transparent conductor oxides. At very high doping concentration, we find a possible "inverse" Moss-Burstein shift, where the apparent band gap decreases with increasing carrier concentration.

DOI: 10.1103/PhysRevB.71.125129 PACS number(s): 71.20.Nr, 61.50.−f

I. INTRODUCTION

Post-transition-metal oxides and their alloys have some unique physical properties. Despite their large band gaps (>3 eV), thus transparent under normal conditions, they can sustain a high concentration of electrons with a high carrier mobility. They are, thus, used as transparent conducting oxides (TCO's) in optoelectronic devices such as flat-panel displays, windshield defrosters, and solar cells.[1,2] The most commonly used post-transition-metal oxides are ZnO, Sn_2O, and In_2O_3 and their alloys. However, the recent growing demand for high-performance and low-cost TCO's (Refs. 3 and 4) has led to an extensive search for new TCO materials with higher transparency and conductivity.[5–13] Among many binary and ternary oxides, $SnZn_2O_4$, $SnCd_2O_4$, and $CdIn_2O_4$ have emerged as promising TCO's. $SnCd_2O_4$ was found to have a high carrier mobility[6,7] compared to most conventional TCO's. $SnZn_2O_4$ has better optical transparency than $SnCd_2O_4$ and does not suffer from the toxicity problem associated with Cd in $SnCd_2O_4$, although its electrical conductivity is lower[6] than that of $SnCd_2O_4$. Recently, the use of $SnCd_2O_4/SnZn_2O_4$ as transparent conducting layers in CdTe solar cells has resulted in the highest cell efficiency achieved to date for this system.[8] $CdIn_2O_4$, on the other hand, is also known for its high *n*-type dopability,[9] with a carrier concentration as high as 10^{21} cm^{-3}.

These ternary compounds have a general chemical formula AB_2O_4 and usually exist in either the cubic spinel structure or an orthorhombic structure, according to the growth conditions. Many experimental and theoretical studies have been carried out to understand the structural, electrical, and optical properties of these three ternary compounds.[6,8,10–12] For example, it is known that $CdIn_2O_4$ is possibly more stable in the normal spinel structure,[10,12,13] whereas $SnZn_2O_4$ and $SnCd_2O_4$ are more stable in the inverse spinel structure.[8,10] $SnCd_2O_4$ has also been grown in the orthorhombic bulk structure.[1,14] However, many physical properties of these compounds are still unknown. For example, their band structure is not well established yet, and the reasons for their combined transparency and conductivity are still under intense debate. More importantly, the relationship between the crystal structure and the electro-optical properties of these compounds has not been well studied. Understanding these issues is of great importance for future design of better TCO materials.

Using the first-principles band structure and total energy methods, we have studied the structural, electronic, and optical properties of $SnZn_2O_4$, $SnCd_2O_4$, and $CdIn_2O_4$. In particular, we have investigated the relationship between the crystal structure and the combined transparency and *n*-type conductivity in these ternary compounds. We find that, in agreement with experiment, $SnZn_2O_4$, $SnCd_2O_4$, and $CdIn_2O_4$ are more stable in the inverse spinel, orthorhombic, and normal spinel structures, respectively. All three compounds have their conduction band minimum (CBM) at the Γ point. The most stable structures of $SnCd_2O_4$ and $CdIn_2O_4$ have indirect band gaps, although the energy differences between the direct and indirect band gaps are small, within a few tens of meV. $SnZn_2O_4$, on the other hand, has a direct band gap. However, we find that, because these structures have inversion symmetry and the valence band maximum (VBM) and the CBM states at Γ have the same parity, the dipole optical transitions are not allowed between states at

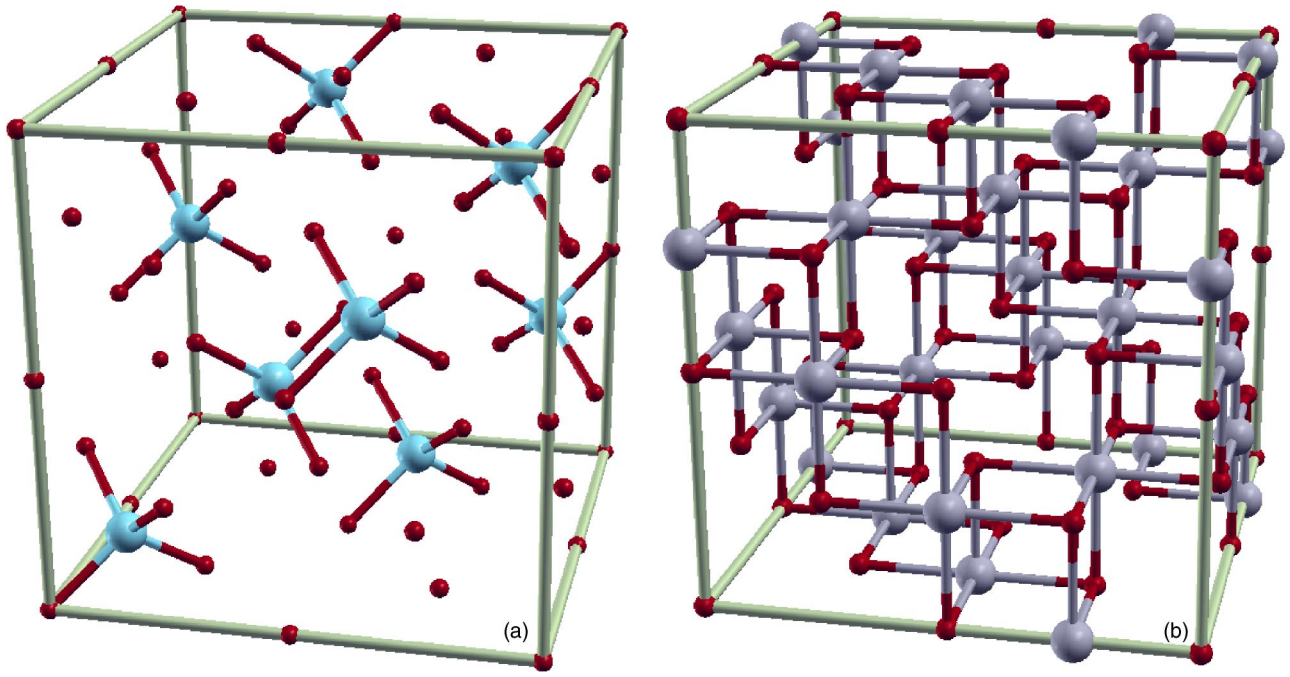

FIG. 1. (Color online) Ball and stick representation of the normal AB_2O_4 spinel structure, showing the position of the O atoms (small balls), bonded to (a) the *A* atoms (large balls) at the tetrahedral sites and (b) bonded to the *B* atoms (large balls) at the octahedral sites.

the zone center. Consequently, the optical band gaps of these materials are usually about 1.0 eV larger than the fundamental band gap. The energy separation between the first and second conduction bands is also large for these compounds in their respective ground states, which explains the transparency observed in these degenerate *n*-type TCO's. The calculated electron effective masses increase with the band gap, as one would expect for conventional semiconductors. Due to the nonparabolicity of the conduction band, we find that the effective mass generally increases as a function of increasing electron concentration or Fermi energy. Moreover, our calculated dependence of the absorption spectrum on the carrier concentration reveals that for heavily doped *n*-type TCO's, a "negative" Moss-Burstein shift is possible, where the apparent band gap decreases with increasing concentration. Our study revealed the characters of the VBM and CBM states, which provides a guideline for future design of suitable TCO materials.

II. METHOD OF CALCULATIONS

The band structure calculations are performed using the local density approximation (LDA),[15,16] with the Ceperley-Alder exchange-correlation potential,[15] as parametrized by Perdew and Zunger.[16] The Kohn-Sham Hamiltonian is solved in a projected augmented-wave[17] (PAW) basis set, as implemented in the VASP code.[18] The *d* electrons are explicitly included in the valence electrons for Cd, Zn, Sn, and In. We perform the calculations with a $2\times2\times2$ Monkhorst-Pack mesh[19] for the normal and inverse spinel structures and with a $4\times4\times2$ Monkhorst-Pack mesh for the orthorhombic structure. We find that the calculated results are converged with respect to the **k**-point sampling. We calculate the optical transition matrix elements $\langle\psi_i|\hat{\mathbf{p}}_\alpha|\psi_f\rangle$ between states *i* and *f* following the method proposed by Adolph *et al.*[20] for a PAW basis set, where $\hat{\mathbf{p}}_\alpha$ is the momentum operator with polarization α and ψ is the PAW (all-electron) wave function. From the transition matrix elements, we derive the imaginary part of the dielectric function according to[21]

$$\mathrm{Im}\ \epsilon_{\alpha\beta}(\omega) = \left(\frac{2\pi e}{m\omega}\right)^2 \sum_{i,f} \int d\mathbf{k} \langle\psi_i|\hat{\mathbf{p}}_\alpha|\psi_f\rangle\langle\psi_f|\hat{\mathbf{p}}_\beta|\psi_i\rangle \delta(E_f(\mathbf{k}) - E_i(\mathbf{k}) - \hbar\omega), \quad (1)$$

where the tetrahedron method[22] is used to perform the integration, with a finer Monkhorst-Pack mesh of up to $10\times10\times10$ divisions. The absorption coefficient is then obtained by

$$A_{\alpha\alpha}(\omega) = \frac{\omega\sqrt{2[|\epsilon_{\alpha\alpha}(\omega)| - \mathrm{Re}\ \epsilon_{\alpha\alpha}(\omega)]}}{c}, \quad (2)$$

where Re $\epsilon_{\alpha\beta}$ is the real part of the dielectric tensor obtained from the imaginary part Im $\epsilon_{\alpha\beta}$ through the Kramers-Kronig relations.[21]

III. CRYSTAL STRUCTURE

In the "normal" spinel structure with space group $Fd\bar{3}m$ (O_h^7), one-eighth of the tetrahedral voids in a face-centered-cubic (fcc) close-packed oxygen sublattice are occupied by *A* atoms [see Fig. 1(a)] and one-half of the octahedral voids are occupied by *B* atoms [see Fig. 1(b)]. There exists also an "inverse" spinel structure, where the tetrahedral voids are occupied by *B* atoms and the octahedral voids are occupied randomly by an equal number of *A* and *B* atoms.[10]

TABLE I. Calculated structural parameters and total energy of $SnZn_2O_4$, $SnCd_2O_4$, and $CdIn_2O_4$ in the normal (*N*), inverse (*I*), and orthorhombic (*O*) structures. The energies are referred to those of the normal spinel. The internal structural parameters of the orthorhombic structures are given in Table II.

		a,b,c (Å)	u	E^{tot} (eV)
$SnZn_2O_4$	*N*	8.55	0.383	0.00
	I	8.58	0.383	−0.68
	O	3.22 5.10 9.29		−0.61
$SnCd_2O_4$	*N*	9.12	0.375	0.00
	I	9.14	0.388	−0.71
	O	3.15 5.48 9.79		−1.00
$CdIn_2O_4$	*N*	9.12	0.388	0.00
	I	9.09	0.381	0.45
	O	3.12 5.57 9.68		0.50

The normal spinel crystal structure is determined by two parameters: the lattice constant a and the anion displacement u. The bond length between the A atom at the center of a AO_4 tetrahedron and its four nearest-neighbor oxygen atoms is given by[10]

$$R_{tetra} = \sqrt{3}(u - 0.25)a, \tag{3}$$

whereas the bond length between the B atoms at the corner of a octahedron and their six nearest oxygen atoms is

$$R_{octa} = \sqrt{(u - 0.625)^2 + 2(u - 0.375)^2}a. \tag{4}$$

The inverse spinel structure is modeled using a small special quasirandom structure (SQS), which has the same lattice vectors as the normal spinel.[10] The effective u parameter in the inverse spinel structure is obtained using the averaged tetrahedral and octahedral bond lengths and the formula given above.

In the orthorhombic structure with space group *Pbam* (D_{2h}^9), the A atom is in a slightly distorted octahedral ($2a$) site with six ($4+2$) A-O bonds, whereas the B atom is in a lower symmetry ($4h$) site and can form either four, six, or eight A-O bonds. For the orthorhombic structure, three external and six internal structural parameters determine the atomic positions.

For each of the $SnZn_2O_4$, $SnCd_2O_4$, and $CdIn_2O_4$ compounds investigated, the calculated equilibrium lattice constants and the internal parameters for the normal spinel, the inverse spinel, and the orthorhombic structures are shown in Tables I and II. We also list in Table I the corresponding total energies referred to the normal spinel structure for the structures considered. For the spinel structure, our calculated results are in good agreement with the all-electron full-potential linearized augmented plane-wave (FLAPW) calculation,[10] as well as with the available experimental data,[1,10,12] with a maximum difference of about 1% only for the Zn compounds. For the orthorhombic $SnCd_2O_4$, our results are also in good agreement with experimental data.[14] We find that, in general, the normal and inverse spinel structures have very similar volumes. However, due to the larger cation coordination, the orthorhombic structure has a slightly smaller volume.

TABLE II. Atomic coordinates for orthorhombic $SnZn_2O_4$, $SnCd_2O_4$, and $CdIn_2O_4$.

	Atom	Site	x	y	z
$SnZn_2O_4$	Sn	2*a*	0.0	0.0	0.0
	Zn	4*h*	0.010	0.326	0.5
	O(1)	4*h*	0.144	0.122	0.5
	O(2)	4*g*	0.186	0.375	0.0
$SnCd_2O_4$	Sn	2*a*	0.0	0.0	0.0
	Cd	4*h*	0.060	0.324	0.5
	O(1)	4*h*	0.238	0.038	0.5
	O(2)	4*g*	0.366	0.307	0.0
$CdIn_2O_4$	In	2*a*	0.0	0.0	0.0
	(Cd,In)	4*h*	0.058	0.331	0.5
	O(1)	4*h*	0.262	0.031	0.5
	O(2)	4*g*	0.371	0.283	0.0

We show in Table III the calculated tetrahedral R_{tetra} and octahedral R_{octa} bond lengths between the cation and oxygen atoms in $SnZn_2O_4$, $SnCd_2O_4$, and $CdIn_2O_4$. We remark that the bond lengths increase as the cation valence decreases or as the atomic number increases. Moreover, Sn and Zn have similar bond lengths, which are smaller than those of Cd. We observe that the octahedral bond length R_{octa} is systematically larger by about 0.1 Å than the tetrahedral R_{tetra} bond length, due to the larger space available at the octahedral site. In the orthorhombic structures, the bond lengths depend on the nearest-neighbor coordination and are very similar to those found in the stable post-transition-metal binary compounds SnO_2, CdO, ZnO, and In_2O_3. We find that the atomic positions in orthorhombic $SnZn_2O_4$ are significantly different than those in orthorhombic $SnCd_2O_4$, because the Zn atom tends to form fourfold bonds, as in ZnO. On the other hand, Cd and Sn prefer to be in a sixfold-coordinated site, as in

TABLE III. Calculated tetrahedral R_{tetra} and octahedral R_{octa} bond lengths between the cations and their oxygen nearest neighbors, for normal and inverse spinel $SnZn_2O_4$, $SnCd_2O_4$, and $CdIn_2O_4$, and averaged nearest-neighbor bond lengths for the orthorhombic structures. The coordination number z in the orthorhombic structure is also quoted. In the last column, we show the calculated cation-oxygen bond lengths $R_{PTM}^{C\text{-}O}$ for the post-transition-metal oxides SnO_2, CdO, ZnO, and In_2O_3.

	Bond	R_{tetra} (Å)	R_{octa} (Å)	$R_{ortho}^{C\text{-}O}$ (Å)/z	$R_{PTM}^{C—O}$ (Å)
$SnZn_2O_4$	Sn—O	1.970	2.067	2.060/6	2.06
	Zn—O	1.975	2.082	1.933/4	1.95
$SnCd_2O_4$	Sn—O	1.980	2.087	2.063/6	2.06
	Cd—O	2.175	2.260	2.300/6	2.33
$CdIn_2O_4$	Cd—O	2.180	2.267	2.308/6	2.33
	In—O	2.070	2.170	2.168/6	2.18

TABLE IV. Structure factor of normal and inverse $SnCd_2O_4$, $SnZn_2O_4$, and $CdIn_2O_4$ spinels. $\vec{G}$ is the reciprocal lattice vector in units of $2\pi/a$.

		$SnCd_2O_4$		$SnZn_2O_4$		$CdIn_2O_4$	
$\vec{G}$	$\lvert\vec{G}\rvert$	N	I	N	I	N	I
1 1 1	1.73	25	35	5	40	35	30
0 0 2	2.00	0	0	0	0	0	0
0 2 2	2.83	86	84	85	51	84	84
1 1 3	3.32	138	135	105	98	136	137
2 2 2	3.46	109	115	50	83	114	112
0 0 4	4.00	117	120	56	119	121	119
1 3 3	4.36	19	16	13	24	15	17
0 2 4	4.47	0	0	0	0	0	0
2 2 4	4.90	73	68	71	41	69	71
3 3 3	5.20	118	105	83	76	106	112
1 1 5	5.20	119	126	96	90	127	123
0 4 4	5.66	232	226	174	173	228	230
1 3 5	5.92	17	25	6	28	24	20

CdO and SnO_2. Furthermore, we find that the atomic coordinates of orthorhombic $CdIn_2O_4$ are very similar to those of orthorhombic $SnCd_2O_4$, except that half of the In atoms occupy the $(2a)$ positions, whereas another half of In and Cd atoms occupy the $(4h)$ sites, leading to a kind of "inverse" orthorhombic structure (see Table II).

From the calculated total energy shown in Table I, we conclude that the inverse and normal spinel structures are the most stable phases of bulk $SnZn_2O_4$ and $CdIn_2O_4$, respectively, and that the orthorhombic structure is mostly favored for bulk $SnCd_2O_4$. The relative stability between the normal and inverse spinel structures can be explained[10] by the Coulomb interaction and by the tendency for Zn to form fourfold covalent bonds. We find that the high valent atoms Sn and In prefer to be in a high-coordination-number (octahedral) site, whereas Zn is preferentially located at the fourfold-coordinated tetrahedral site. Similar arguments can be used to explain the stability of the orthorhombic structure.

To help in distinguishing between the normal and inverse spinel structures in x-ray diffraction (XRD) measurements, we have also calculated the structure factors of $SnZn_2O_4$, $SnCd_2O_4$, and $CdIn_2O_4$, in the normal and inverse spinel structures, using the all-electron FLAPW method.[23] The results are shown in Table IV. We find that the structure factors are quite different for the normal and inverse spinel structures of $SnZn_2O_4$. They can be, therefore, easily distinguished in XRD measurements, where the XRD intensity is proportional to the structure factors squared. On the other hand, in the cases of $SnCd_2O_4$ and $CdIn_2O_4$, the structure factor for the normal and inverse structures are similar because the atomic number of Cd, In, and Sn are comparable. This makes the identification of the structure using XRD difficult. It is also interesting to notice that the structural factor of $SnCd_2O_4$ in the inverse spinel structure $[Cd(Sn,Cd)O_4]$ is very similar to that of $CdIn_2O_4$ in the normal spinel structure. This stems from the fact that the average atomic number of Sn and Cd at the octahedral site of the $[Cd(Sn,Cd)O_4]$ inverse spinel structure is the same as that of In at the octahedral site of the $CdIn_2O_4$ normal spinel structure.

IV. BAND STRUCTURE

A good performing *n*-type TCO must simultaneously satisfy two requirements: (i) large optical band gap, as well as large energy separation between the CBM and the second conduction band (SCB), for transparency; (ii) a low CBM with respect to the vacuum level, for high dopability, as well as a small effective mass, for good conductivity. As a consequence of the second condition, a low VBM, which is a common characteristic of oxides, is also required to meet the first condition. In the following, we will show the results of our study on the band structures of $SnZn_2O_4$, $SnCd_2O_4$, and $CdIn_2O_4$, focusing on the VBM, CBM, and SCB states, and identify general trends for these types of materials.

A. $SnZn_2O_4$

We show in Fig. 2(a) the band structure of $SnZn_2O_4$ along the L-Γ-X line for the normal and inverse spinel structures and along the X-Γ-Z line for the orthorhombic structure. In Fig. 3(a) we plot the atom- and angular-momentum-resolved local density of states (LDOS) of $SnZn_2O_4$ in the normal structure. Only the dominant components of the LDOS are shown. The inverse and orthorhombic structures show very similar features at the vicinity of the band gap edges and are not shown here. We find that the top of the valence band consists predominantly of the cation *d* and O *p* states, which hybridize strongly, whereas the bottom of the conduction bands arises mostly from the mixture of oxygen and cation *s* states.

Further analysis shows that in the spinel structure with the O_h space group, the local oxygen site has a C_{3v} symmetry, whereas the tetrahedral and octahedral sites have the local T_d and D_{3d} symmetry, respectively. At the Γ point, (a) the VBM state has the Γ_{12v} representation and consists mostly of O *p* and cation *d* states of the octahedral site, with some *d* character from the cation at the tetrahedral site [Fig. 4(b)]. (b) The CBM state has the Γ_{1c} representation, with predominantly O *s* and cation *s* states of the tetrahedral site, as well as some *s* character from the cation at the octahedral site [Fig. 4(c)]. A minority of O *p* and Zn *d* characters can be also observed for this state. (c) The SCB state has the $\Gamma_{2'c}$ representation and consists of O *s* and *p*, of cation *s* states of the tetrahedral site only, as well as of some *p* state from the cation at the octahedral site [Fig. 4(d)]. With this analysis, we can now explain the change in the band gap and the splitting between the first two conduction bands, $E_{12}=E_{SCB}-E_{CBM}$, as a function of the crystal structures.

The results for E_g and E_{12} are listed in Table V. We find that when $SnZn_2O_4$ changes from the normal to the inverse spinel structure—i.e., when Sn and half of the Zn change sites—both the band gap and E_{12} increases. When Sn is at the octahedral site, the VBM energy decreases, which is due to the lower Sn 4*d* orbital energy compared to that of the Zn

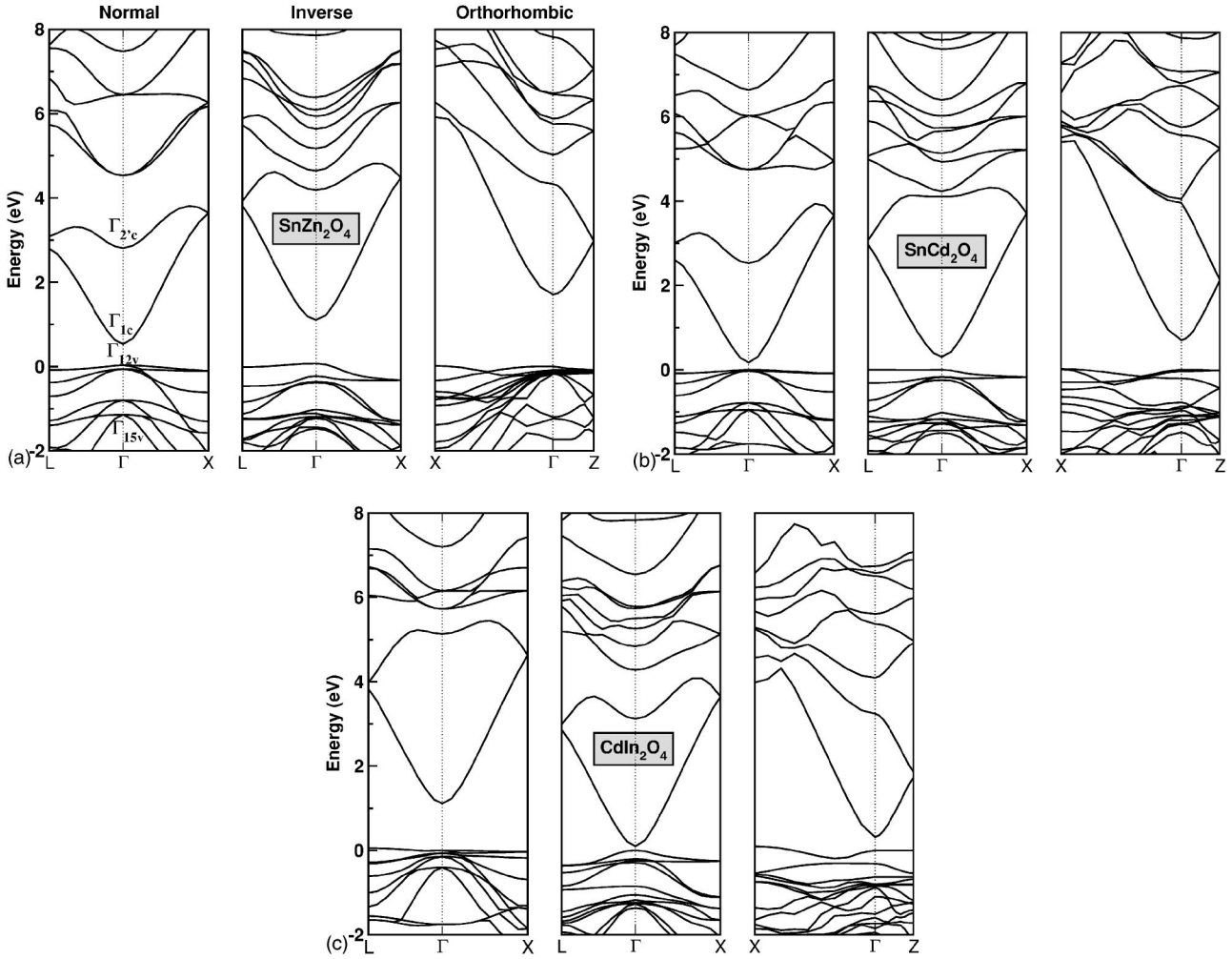

FIG. 2. Band structure of $SnZn_2O_4$ (upper panel), $SnCd_2O_4$ (middle panel), and $CdIn_2O_4$ (lower panel), in the normal and inverse spinel structure, along the L-Γ-X line, and in the orthorhombic structure, along the X-Γ-Z line. The zero of the energy is set at the top of the valence band at Γ. We do not correct for the LDA band gap error, which is estimated to be about 1.4 eV. Some important states at Γ are labeled in the normal spinel structure of $SnZn_2O_4$.

3*d* orbital and, hence, the reduced *p*-*d* repulsion at the octahedral site [see (a) above]. Moreover, because Zn has a much higher 4*s* orbital energy than the Sn 5*s* orbital, both of the first two conduction bands energies increase. However, the energy of the SCB increases more than that of the CBM state because the former contains only Zn 4*s* orbital but no Sn 5*s* orbital [see (b) and (c) above]. This explains why the fundamental band gap E_g as well as E_{12} of $SnZn_2O_4$ is much larger in the inverse spinel structure than in the normal spinel structure.

We find that the orthorhombic $SnZn_2O_4$ structure has an even larger band gap than the inverse spinel structure. However, the E_{12} energy separation is smaller than that in the inverse spinel structure, but larger than that in the normal spinel structure. Due to the smaller volume of the orthorhombic structure compared to that of the spinel structure, the CBM in orthorhombic structure has a higher energy.[24] Furthermore, the *p*-*d* coupling is reduced at the VBM, which is due to the lower symmetry of the orthorhombic structure. This explains the larger band gap of the orthorhombic structure compared to the spinel structure. Moreover, we find that, in contrast to the spinel structure, the SCB state has a mixed Zn 4*s* and Sn 5*s* character in the orthorhombic structure. Therefore, the energy separation E_{12} in the orthorhombic structure is in between that of the normal and the inverse spinel structure [see (c) above].

B. $SnCd_2O_4$

The band structure and the LDOS of the normal spinel $SnCd_2O_4$ are shown in Figs. 2(b) and 3, respectively. The variation of the band gap and the changes in E_{12} are similar to those in $SnZn_2O_4$ and can be explained in an analogous way to that described above for $SnZn_2O_4$. The only noticeable distinctions between $SnCd_2O_4$ and $SnZn_2O_4$ are that the band gap of $SnCd_2O_4$ is smaller than that of $SnZn_2O_4$, due mostly to the smaller volume of $SnZn_2O_4$, and that the difference in the band gap between the three structures is smaller in $SnCd_2O_4$ than in $SnZn_2O_4$. This can be explained by the fact that the atomic size of Cd is much larger than that of Zn and Sn, whereas Sn and Zn have similar atomic sizes. When Cd moves to the tetrahedral site in the $SnCd_2O_4$ in-

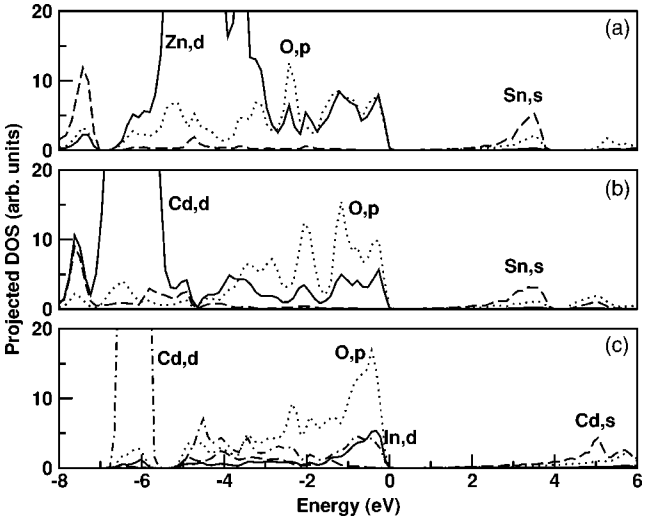

FIG. 3. Projected DOS of (a) $SnZn_2O_4$, (b) $SnCd_2O_4$, and (c) $CdIn_2O_4$ in the normal spinel structure. The tops of the valence band at Γ are aligned for easy comparison. The *A s*, O *p*, and *B d* components are the most significant in the range plotted, along with the O *s* state in the vicinity of the conduction band minimum, which is not shown for clarity.

verse spinel structure, the tetrahedral bond length increases, whereas the octahedral bond length decreases, as reflected by the different *u* parameters observed for the normal and inverse spinel structures (see Table I). Consequently, this lowers the energy of the CBM state, which is an antibonding state centered mostly on the tetrahedral site [see (b) above], and increases the VBM energy, due to the large *p-d* coupling at the octahedral site [see (a) above]. Thus, the strain-induced deformation effect partially cancels the chemical effect in $SnCd_2O_4$, which explains the smaller band gap variation in $SnCd_2O_4$.

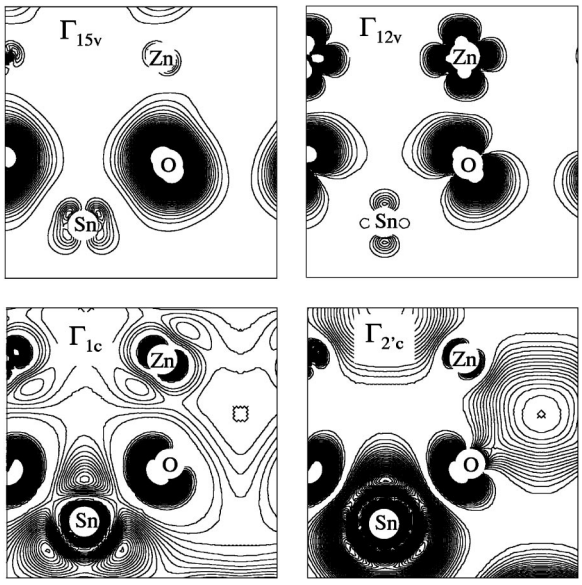

FIG. 4. Contour plot of the charge density, in the (110) plan of the normal spinel $SnZn_2O_4$, for the Γ_{15v} state, the VBM (Γ_{12v}) state, the CBM (Γ_{1c}) state, and the second conduction band state ($\Gamma_{2'c}$).

C. $CdIn_2O_4$

The band structure of $CdIn_2O_4$ is plotted in Fig. 2(c), and the LDOS of $CdIn_2O_4$ in the normal structure is shown in Fig. 3. In contrast to $SnZn_2O_4$ and $SnCd_2O_4$, the hybridization between the O *p* and the cation *d* states at the octahedral site is much smaller in the normal spinel $CdIn_2O_4$, which is due to the lower 4*d* orbital energy of In compared to that of the Zn 3*d* and Cd 4*d* states. The band gap of $CdIn_2O_4$ is found to be slightly indirect in the normal spinel and the orthorhombic structures, but is direct in the inverse spinel structure. The top of the valence band is at the *L* point for the normal spinel and at the *X* point for the orthorhombic structure. The difference between the direct band gap of normal spinel $CdIn_2O_4$ at Γ and its indirect band gap is only 0.05 eV, and it is 0.09 eV in the orthorhombic structure. This very small difference can hardly be resolved experimentally, and a direct band gap has been suggested for normal spinel $CdIn_2O_4$.[25]

In the case of $CdIn_2O_4$, we observe a different trend in the band gap variation and E_{12} energy separation compared to that of $SnZn_2O_4$ and $SnCd_2O_4$; i.e., the band gap decreases from normal to inverse spinel and then increases slightly in the orthorhombic structure. In the inverse spinel structures of $SnZn_2O_4$ and $SnCd_2O_4$, a low-valence atom (Zn or Cd) occupies the tetrahedral site and a high-valence atom (Sn) is at the octahedral site. In contrast, in the inverse spinel structure of $CdIn_2O_4$, the high-valence atom (In) occupies the tetrahedral site and the low-valence atom (Cd) is at the octahedral site. Therefore, the trends observed in $SnZn_2O_4$ and $SnCd_2O_4$ due to (a), (b), and (c) above are reversed in $CdIn_2O_4$. The slightly increased band gap of the orthorhombic structure relative to the inverse spinel structure is again due to the smaller volume structure and the reduced *p-d* coupling in the orthorhombic structure.

As mentioned above, the normal spinel $CdIn_2O_4$ is very much like the inverse spinel $SnCd_2O_4$ [$Cd(Sn,Cd)O_4$]. However, the band gap of normal $CdIn_2O_4$ is much larger than that of inverse $SnCd_2O_4$. This is because when In converts to Sn+Cd, the CBM becomes more localized on the Sn atom, which has a lower *s*-orbital energy than that of In. Furthermore, the O *p* and Cd *d* coupling is much larger than that of O *p* and In *d*. Therefore, the CBM (VBM) of the inverse spinel $SnCd_2O_4$ is lower (higher) than that of the normal spinel $CdIn_2O_4$, resulting in a smaller band gap for the former compared to the latter.

D. General implications for TCO's

Based on the analysis above on the atomic characteristics of the band edge states and on the effects of the volume deformation on the CBM and VBM levels, we propose here some general rules, which should be considered in designing TCO's with better transparency and higher carrier concentration. (i) To create materials with a low CBM and thus high dopability and conductivity, the cations should have relatively large atomic size, because a large crystal volume results in a lower CBM energy and low-lying *s* orbital, especially at the tetrahedral sites. A split character at the octahedral site can also lower the CBM. (ii) To achieve a low

TABLE V. Calculated fundamental band gap E_g, optical band gap E_g^{opt}, energy difference E_{12} between the first and second conduction bands, and electron effective mass of $SnZn_2O_4$, $SnCd_2O_4$, and $CdIn_2O_4$ in the normal (*N*), inverse (*I*), and orthorhombic (*O*) structures. E_g, E_g^{opt}, and E_{12} are calculated at the Γ point. Available experimental data are shown in parentheses. The estimated LDA band gap error is about 1.4 eV. Three different values are shown for the effective masses of the nonisotropic orthorhombic structure. The *z* axis of the orthorhombic structure is chosen to be parallel to the largest lattice parameter. Due to the LDA band gap error, the calculated effective masses are also underestimated by about $0.05m_0$.

		E_g (eV)	E_g^{opt} (eV)	E_{12} (eV)	m^* (m_0)
	N	0.50	1.67	2.28	0.188
$SnZn_2O_4$	*I*	1.07	2.20 (3.35[a])	3.08	0.230
	O	1.70	1.70	2.63	0.202 0.173 0.137
	N	0.17	1.13	2.36	0.141
$SnCd_2O_4$	*I*	0.30	1.32	3.80	0.175
	O	0.69	1.47 (2.79[b])	3.26	0.156 0.164 0.126
	N	1.11 (2.23[b])	1.52 (3.28[b])	4.02	0.168
$CdIn_2O_4$	*I*	0.09	1.27	3.02	0.151
	O	0.32	1.13	2.92	0.131,0.147,0.107

[a]Reference 31.
[b]Reference 25.

VBM and thus the high band gap necessary for transparency, the *d*-orbital binding energy of the cations should be large, especially at the octahedral sites, in order to yield a small *p*-*d* coupling. (iii) To obtain a high SCB level relative to the CBM level and improve transparency, a large energy difference between the *s* orbitals of the cation at the tetrahedral site and that at the octahedral site is required. Finally, (iv) to stabilize the compound, the high-valence cation should occupy the octahedral site and the low-valence atom the tetrahedral site. These general considerations suggest that the inverse spinel $SnCd_2O_4$ would have better conductivity, whereas the inverse spinel $SnZn_2O_4$ and the normal spinel $CdIn_2O_4$ would have better transparency.

V. EFFECTIVE MASS

As mentioned above, a good TCO should have a small electron effective mass, to yield a high conductivity. The calculated electron effective masses at the Γ point of the CBM are shown in Table I. The electron effective mass is quite isotropic for the spinel compounds, but nonisotropic for the orthorhombic structure. In this case, the *z* axis of the orthorhombic structure is chosen to be parallel to the largest lattice constant. We find that in the case of $SnZn_2O_4$ and $SnCd_2O_4$, the effective mass is larger in the inverse spinel structure than in the normal spinel, due to the higher band gap of the inverse spinel. The opposite trend is observed for $CdIn_2O_4$, for which the normal spinel structure has a larger effective mass than the inverse spinel structure, which is consistent with the fact that the normal spinel structure has a large band gap. In the orthorhombic structure, the effective mass is nonisotropic and greatly depends on the direction considered. We find that the effective mass is smallest in the *z* direction for the three systems studied. Therefore, for the orthorhombic structure, the conductivity should be larger in the direction parallel to the largest lattice parameter. We would also like to point out that due to the underestimation of the band gap by the LDA, the calculated effective mass is underestimated compared to experiment. We estimate that the error in our calculated effective mass is about $0.05m_0$, where m_0 is the free-electron mass.

Most TCO's contain a high concentration of electrons in the conduction band. This results in the Moss-Burstein shift (increase) (Refs. 26 and 27) of the band gap[31] as the carrier concentration is increased. Moreover, as the conduction band is nonparabolic,[31] the effective mass also depends on the Fermi energy. We have studied these effects in $SnZn_2O_4$, $SnCd_2O_4$, and $CdIn_2O_4$ by calculating the effective mass away from the Brillouin zone center, as a function of the carrier concentration, for normal and inverse spinel structures. In our analysis, we assume that the character of the CBM state is not changed by electronic occupation. We calculate the effective masses in two different ways. As a first definition, we derive a "transport" effective mass by assuming that the first derivative of the conduction band energy $E(k)$ is equal to that of a parabolic band at the same *k* point. Therefore, the transport effective mass $m_T^*(E)$ can be defined by

$$\frac{1}{m_T^*(E)} = \frac{1}{\hbar^2 k}\frac{dE}{dk}. \tag{5}$$

To describe the nonparabolicity of the conduction band, Young *et al.*[28] used the expression

$$\frac{\hbar^2 k^2}{2m_0^*} = \gamma(E), \tag{6}$$

where m_0^* is the effective mass at the minimum of the conduction band and $\gamma(E)$ is a function of the energy. Taking the

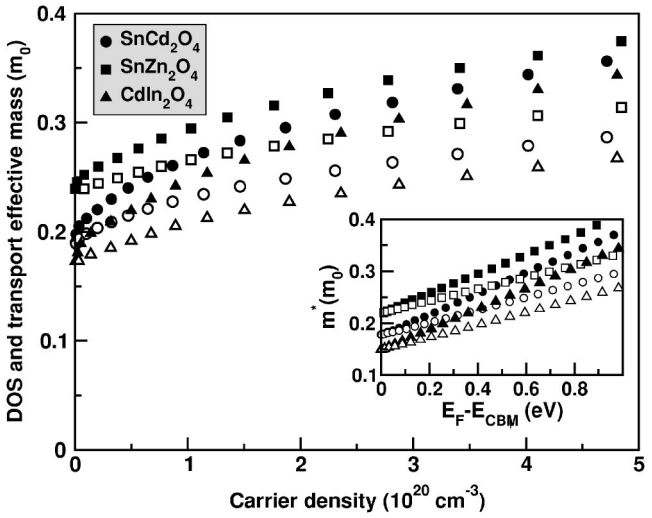

FIG. 5. DOS (open symbols) and transport (solid symbols) effective masses calculated as a function of the carrier concentration for $SnCd_2O_4$, $SnZn_2O_4$, and $CdIn_2O_4$ in the inverse spinel structure. We plot in the inset the effective masses as a function of the Fermi level E_F, calculated from the conduction band minimum energy E_{CBM}. We do not correct for the LDA error on the effective mass, which is estimated to be about $0.05m_0$.

derivative of both sides of Eq. (6) with respect to k, we obtain

$$\frac{d\gamma}{dk} = \frac{d\gamma}{dE}\frac{dE}{dk} = \frac{\hbar^2 k}{m_0^*}. \tag{7}$$

From Eqs. (5) and (7) above we arrive at

$$m_T^*(E) = m_0^* \frac{d\gamma}{dE}, \tag{8}$$

which is the formula used by Young *et al.*[28] This approach should be compared to the experimentally measured effective mass derived from transport properties.[28]

In the second approach, we assume equality between the number of states up to energy E obtained from our band structure calculations and that obtained from a parabolic energy dispersion, for which the effective mass is constant. This DOS effective mass $m_{DOS}^*(E)$ is thus calculated from

$$m_{DOS}^{*3/2}(E)\int_0^E \sqrt{E'}dE' = \int_0^E m_T^{*3/2}(E')\sqrt{E'}dE', \tag{9}$$

where E is measured from the conduction band minimum. The effective mass $m_T^*(E)$ in Eq. (9) is obtained from the first derivative (gradient) of the conduction band energy with respect to the wave vector k, as required by the density-of-states calculation, and is given in Eq. (5).

We show in Fig. 5 the results for m_{DOS}^* and $m_T^*(E)$ as a function of the carrier concentration and the Fermi level for $SnZn_2O_4$, $SnCd_2O_4$, and $CdIn_2O_4$ in the inverse spinel structure. The curves in Fig. 5 clearly show that the conduction bands of these compounds are nonparabolic. The degree of nonparabolicity can be estimated from Eq. (6) by assuming an energy expansion of the form[28]

$$\gamma(E) = E + \frac{E^2}{E_1}, \tag{10}$$

where E_1 is a constant. For the normal spinel structures, we find that E_1 increases from 1.33 to 1.59 and 1.75 eV, from $SnCd_2O_4$ to $SnZn_2O_4$ and $CdIn_2O_4$, respectively. E_1 is larger in the inverse structures of $SnCd_2O_4$ and $SnZn_2O_4$ compared to the normal ones. The opposite is true for $CdIn_2O_4$, because large E_1 corresponds to smaller nonparabolicity. The results indicate that the degree of nonparabolicity increases with decreasing band gap. This can be understood by noticing that in semiconductors, the nonparabolicity is caused by a coupling between the conduction band and the light-hole valence band states, which decreases with larger band gap.

The experimental results[6,11,30] on the effective masses of TCO's are not very clear. A constant electron effective mass has been reported for $CdIn_2O_4$ up to a Fermi energy of 1 eV.[11] In the case of $SnCd_2O_4$, the electron effective mass has been found to increase,[29] to be constant,[6] or to decrease,[30] as a function of the carrier concentration. Although the effective mass of $SnZn_2O_4$ has been recently reported to increase with increasing carrier concentration, the measured value[29,31] is significantly smaller than that of $SnCd_2O_4$, in contradiction with the expectation that $SnZn_2O_4$ should have a larger effective mass because of its larger band gap. We believe more accurate measurements of the effective masses for these compounds are needed to clarify these issues.

The above discussion is related to the transport effective mass given by Eq. (5). We find that the DOS effective mass is systematically smaller than the transport effective mass. The slope of the change of the effective mass with respect to the energy is calculated to be about 1.65 times larger for the transport mass compared to the DOS mass, for inverse as well as normal spinel structures.

VI. OPTICAL PROPERTIES

A. Transition matrix elements

As mentioned above, TCO's have a relatively large fundamental band gap, which is a necessary condition for good transparency. However, the carrier concentration of heavily n-type doped TCO's can reach 10^{21} cm^{-3}. Due to the Moss-Burstein[26,27] effect, the threshold of the transition may occur at $\mathbf{k}$ points away from the zone center. Furthermore, for heavily doped systems, a transition may also occur between the conduction bands. Therefore, the optical properties of TCO's are determined not only by the optical transitions between the valence bands and the unoccupied states of the conduction bands, but also between the occupied conduction states and the other conduction band states.

We first consider the optical transitions for undoped TCO's. In Fig. 6 we plot the $\mathbf{k}$ dependence of the transition matrix elements squared, P^2, between the top of the valence band and the bottom of the conduction band states, for normal spinel $SnZn_2O_4$, $SnCd_2O_4$, and $CdIn_2O_4$, along the L-Γ-X line. Similar behavior is expected for the inverse spinel systems, which have the same global symmetry as the normal spinel structures. We neglect the spin-orbit coupling

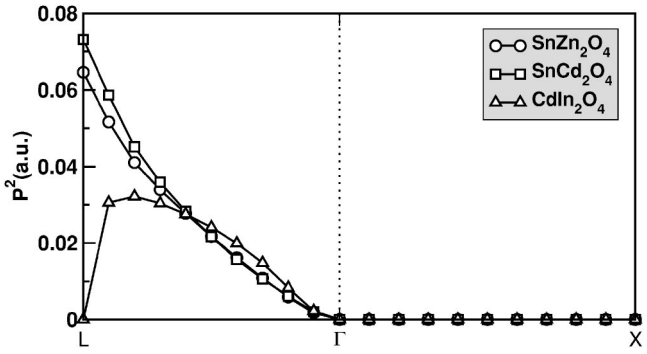

FIG. 6. **k** dependence of the transition matrix elements squared between the top of the valence band and the bottom of the conduction band states, for $SnCd_2O_4$, $SnZn_2O_4$, and $CdIn_2O_4$ in the normal spinel structure, along the L-Γ-X line.

in our analysis. As mentioned above, the VBM state at Γ has the Γ_{12v} representation and is twofold degenerate in the cubic spinel systems, with a O_h point-group symmetry, whereas the CBM state has the Γ_{1c} representation. From group theory, we find that the transition from the VBM to the CBM, which defines the fundamental band gap at Γ, is forbidden, as can be seen from Fig. 6. Furthermore, transitions at Γ are allowed only between the Γ_{1c} state and valence states with a Γ_{15v} representation, which are found to consist mostly of O p and d states of the cation at the tetrahedral site, with some p character from the cation at the octahedral site [see Fig. 4(a)]. Consequently, we find that the measured optical band gap is usually larger by about 1 eV than the fundamental band gap (see Table V). The smaller difference between the Γ_{12v} and Γ_{15v} energies in the normal spinel $CdIn_2O_4$ ($\sim$0.4 eV) is due to the lower energy of the Γ_{12v} state, related to the small p-d coupling of this state.

The symmetry-induced forbidden transition persists for the band edge states along the Γ-X line, which have a reduced D_{4h} symmetry. However, transitions are allowed between states along the Γ-L direction (Fig. 6), which has a reduced D_{3d} symmetry. The transition at L is forbidden in the case of $CdIn_2O_4$, because the two first conduction states switch order compared to the cases of $SnCd_2O_4$ and $SnZn_2O_4$.

The symmetry at the Γ point is D_{2h} for the orthorhombic structure. We find a forbidden transition between the VBM and CBM states at the Γ point in $SnCd_2O_4$ and $CdIn_2O_4$, but an allowed transition for $SnZn_2O_4$ due to a change in the VBM character.

Experimentally, the normal spinel $CdIn_2O_4$ is found[25] to have a forbidden band gap, as obtained from our calculation. However, the optical transition of inverse spinel $SnZn_2O_4$ (Ref. 31) and orthorhombic $SnCd_2O_4$ (Ref. 25) are reported to be allowed, in contradiction to our calculations. This discrepancy can be explained by the fact that the experimental samples are n-type doped TCO's, for which optical transitions occur away from the Γ point, where transitions are indeed allowed by symmetry (Fig. 6).

We should point out that, although our LDA-calculated band gaps are underestimated by about 1.4 eV, our conclusions on the forbidden band gap in the thermodynamically stable inverse spinel $SnZn_2O_4$, orthorhombic $SnCd_2O_4$, and normal spinel $CdIn_2O_4$ are based on symmetry analysis and are, therefore, not affected by the LDA band gap error. We believe more experiments should be carried out to test our predictions.

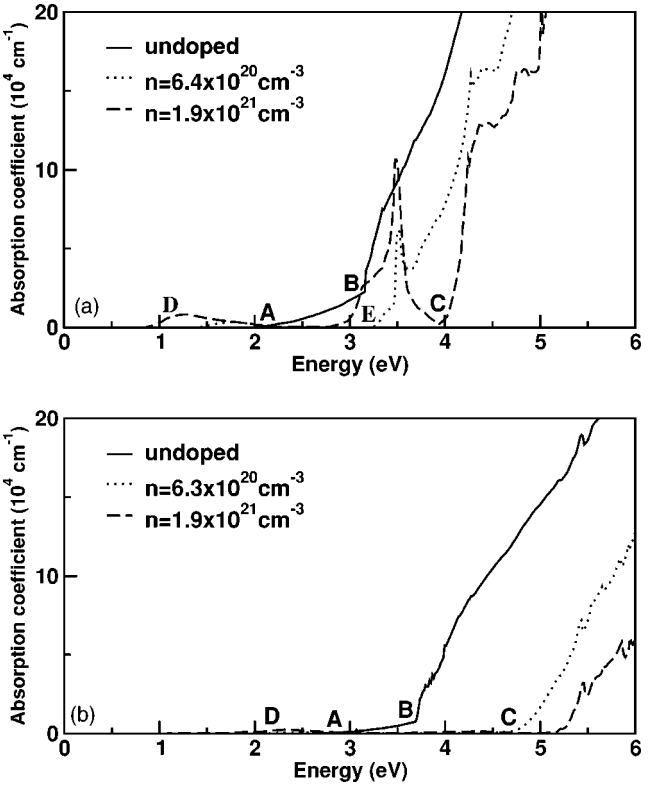

FIG. 7. Variation of the absorption coefficient with the electronic carrier concentration for (a) normal spinel $SnZn_2O_4$ and (b) inverse spinel $SnZn_2O_4$. Features A–E correspond to the transitions indicated in Fig. 8.

Similar to the optical transitions between the VBM and CBM states, we find that transitions between the first and second conduction bands are forbidden at the Γ point in both cubic and orthorhombic structures. For instance, in the cubic spinel structure, the CBM and SCB states have the Γ_{1c} and $\Gamma_{2'c}$ representations, respectively. However, optical transitions are allowed at the Γ point only between the Γ_{1c} and Γ_{15c} states.

B. Absorption coefficient

When the system is n-type doped, optical transitions can occur between the CBM and states with energy higher than the CBM energy, for k points away from the Brillouin zone center. Moreover, an increase in the apparent band gap (Moss-Burstein shift) is expected as a result of transitions from valence band states to unoccupied conduction states away from the Γ point. These two effects are reflected in the absorption coefficient, when the carrier concentration is varied. We choose the $SnZn_2O_4$ compound to illustrate the phenomenon. In Fig. 7(a) we plot the absorption coefficient of normal spinel $SnZn_2O_4$ as a function of the carrier concentration. We apply a constant upward shift of 1.4 eV to the

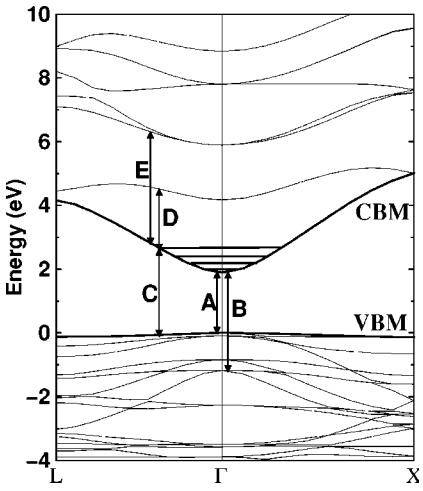

FIG. 8. Transition ($A-E$) observed in the absorption spectrum of normal spinel $SnZn_2O_4$ shown in Fig. 7(a). The occupied levels in the conduction band are also indicated for the *n*-type doped cases.

conduction band energy, which is the approximate difference in energy found between our LDA calculations and the experimental data, on the optical band gap (see Table I). The absorption features are indicated by letters ($A-E$), which correspond to the transitions shown in Fig. 8.

Due to the forbidden transition at Γ, the absorption coefficient starts to increase very slowly at the fundamental band gap threshold (letter *A*) and increases sharply only at a higher energy when the associated matrix elements are large and the transitions are allowed (letter *B*). New features appear when the carrier concentration increases. First, the optical band gap shifts toward higher energy as the carrier concentration increases, related to the Moss-Burstein effect (feature *C*). Moreover, a new peak appears (letter *D*) below the fundamental band gap, whose amplitude increases with the carrier concentration. This absorption is related to allowed transitions between the occupied conduction band and the second conduction band and should reduce the transparency of the TCO's. This indicates that a TCO with good transparency requires a large energy difference between the first and second conduction bands. Furthermore, we find a feature in the absorption spectrum (letter *E*) related to transitions between the first conduction band and other conduction bands with higher energy. In contrast to the *C* transition, the energy of the *E* transition decreases with increasing carrier concentration. As long as the energy of the *C* transition is smaller than that of the *E* transition, the latter will be difficult to resolve in the absorption spectrum. However, at very high concentration, an apparent decrease in the band gap (inverse Moss-Burstein shift) may be observed as the carrier concentration increases. This may also reduce the transparency of the TCO's.

Features *D* and *E* appear to be structure dependent, because they are related to the E_{12} band gap mentioned before. We have already mentioned that E_{12} increases from normal to inverse structure (see Table V). Therefore, in cases where the *C* transitions occur at energies similar to the *E* transition energies, the latter transitions cannot be resolved in the absorption spectrum. Indeed, we find that this feature does not appear in the absorption spectrum of the inverse spinel $SnZn_2O_4$ [see Fig. 7(b)], which has a larger E_{12} than that of the normal spinel structure.

We find a very similar *D* feature in the case of $SnCd_2O_4$ at transition energies of about 1.5 eV, which are lower than the optical band gap energy. The *E* transitions are also observed, typically with energies slightly smaller than those of the *C* transitions. In the case of $CdIn_2O_4$, the *D* and *E* transitions have energies much higher than those of the *C* transitions and are, therefore, not observed in the absorption spectrum.

VII. SUMMARY

We have studied the structure-related electronic and optical properties of $SnZn_2O_4$, $SnCd_2O_4$, and $CdIn_2O_4$ with first-principles band structure and total energy methods. We find that $SnZn_2O_4$, $SnCd_2O_4$, and $CdIn_2O_4$ are more stable in the inverse spinel, orthorhombic, and normal spinel structures, respectively, with indirect band gaps for $SnCd_2O_4$ and $CdIn_2O_4$ and direct for $SnZn_2O_4$. The trends observed in the fundamental band gap and in the energy difference between the first and second conduction bands are explained in terms of chemical and structural effects. We show results on the change in the electron effective mass with the crystal structure and the electron concentration. We find also that the optical transitions are forbidden between the VBM and CBM states at the Γ point and between the first and second conduction bands. Therefore, the optical gaps are usually much larger than the fundamental band gaps. The absorption spectra of these compounds are found to depend strongly on their structures and on the carrier concentration. General rules are proposed to design TCO's according to their atomic characters.

ACKNOWLEDGMENTS

We would like to thank Dr. D. L. Young, Dr. T. J. Coutts, Dr. D. S. Ginley, and Dr. S. B. Zhang for helpful discussions. This work is supported by the U.S. Department of Energy, under Contract No. DE-AC36-99GO10337 to NREL.

[1] R. D. Shannon, J. L. Gillson, and R. J. Bouchard, J. Phys. Chem. Solids **38**, 877 (1977).
[2] See review articles in MRS Bull. **25**, 1 (2000).
[3] K. Nomura, H. Ohta, K. Ueda, T. Kamiya, M. Hirano, and H. Hosono, Science **300**, 1269 (2003).
[4] B. G. Lewis and D. C. Paine, MRS Bull. **25**, 22 (2000).
[5] Y. Dou and G. Egdell, Phys. Rev. B **53**, 15 405 (1996).
[6] T. J. Coutts, D. L. Young, X. Li, W. P. Mulligan, and X. Wu, J.

Vac. Sci. Technol. A **18**, 2646 (2000).
[7] A. J. Nozik, Phys. Rev. B **6**, 453 (1972).
[8] X. Z. Wu, R. Ribelin, R. G. Dhere, D. S. Albin, T. A. Gessert, S. Asher, D. H. Levi, A. Mason, H. R. Moutinho, and P. Sheldon, in *Proceedings of 28th IEEE PVSC* (IEEE, Piscataway, NJ, 2000), p. 470.
[9] K. Budzynska, E. Leja, and S. Skrzypek, Sol. Energy Mater. **12**, 57 (1985).
[10] Su-Huai Wei and S. B. Zhang, Phys. Rev. B **63**, 045112 (2001).
[11] X. Wu, T. J. Coutts, and W. P. Mulligan, J. Vac. Sci. Technol. A **15**, 1057 (1997).
[12] B. Li, L. Zeng, and F. Zhang, Phys. Status Solidi A **201**, 960 (2004).
[13] D. R. Kammler, T. O. Mason, D. L. Young, T. J. Coutts, D. Ko, K. R. Poeppelmeier, and D. L. Williamson, J. Appl. Phys. **90**, 5979 (2001).
[14] M. E. Bowden and C. M. Cardile, Powder Diffr. **5**, 36 (1990).
[15] D. M. Ceperley and B. J. Alder, Phys. Rev. Lett. **45**, 566 (1980).
[16] J. P. Perdew and A. Zunger, Phys. Rev. B **23**, 5048 (1981).
[17] P. E. Blöchl, Phys. Rev. B **50**, 17 953 (1994); G. Kresse and D. Joubert, *ibid.* **59**, 1758 (1999).
[18] G. Kresse and J. Furthmüller, Comput. Mater. Sci. **6**, 15 (1996).
[19] H. J. Monkhorst and J. D. Pack, Phys. Rev. B **13**, 5188 (1976).
[20] B. Adolph, J. Furthmüller, and F. Bechstedt, Phys. Rev. B **63**, 125108 (2001).
[21] P. Y. Yu and M. Cardona, *Fundamentals of Semiconductors*, 2nd ed. (Springer-Verlag, Berlin, 1999).
[22] P. E. Blöchl, Phys. Rev. B **49**, 16 223 (1994).
[23] S.-H. Wei and H. Krakauer, Phys. Rev. Lett. **55**, 1200 (1985).
[24] S.-H. Wei and A. Zunger, Phys. Rev. B **60**, 5404 (1999).
[25] F. P. Koffyberg and F. A. Benko, Appl. Phys. Lett. **37**, 320 (1980).
[26] T. S. Moss, Proc. Phys. Soc. London, Sect. B **67**, 775 (1954).
[27] L. Burstein, Phys. Rev. **93**, 632 (1954).
[28] D. L. Young, T. J. Coutts, V. I. Kaydanov, A. S. Gilmore, and W. P. Mulligan, J. Vac. Sci. Technol. A **18**, 2978 (2000).
[29] D. L. Young, Ph.D. thesis, Colorado School of Mines, 2002.
[30] D. S. Ginley and C. Bright, MRS Bull. **25**, 15 (2000).
[31] D. L. Young, H. Moutinho, Y. Fan, and T. J. Coutts, J. Appl. Phys. **92**, 310 (2002).